Entanglement-enhanced quantum strategies for accurate estimation of multibody-group motion and moving-object characteristics

Yongqiang Li and Changliang Ren*

Key Laboratory of Low-Dimensional Quantum Structures and Quantum Control of Ministry of Education, Key Laboratory for Matter Microstructure and Function of Hunan Province, Department of Physics and Synergetic Innovation Center for Quantum Effects and Applications, Hunan Normal University, Changsha 410081, China and Institute of Interdisciplinary Studies, Hunan Normal University, Changsha 410081, China

(Received 4 July 2023; accepted 15 November 2023; published 7 December 2023)

This study presents a quantum strategy for simultaneous estimation of two physical quantities using different entanglement resources. We explore the utilization of positively or negatively time-correlated photons. The proposed method enables the detection of the central position and relative velocity of multibody systems, as well as precise measurement of the size and velocity of moving objects. Comparative analysis with other strategies reveals the superior quantum advantage of our approach, particularly when appropriate entanglement sources with a high degree of entanglement are employed. These findings contribute to advancing our understanding of quantum strategies for accurate measurements.

DOI: 10.1103/PhysRevA.108.062605

I. INTRODUCTION

Quantum metrology [1–6] is an emerging application of quantum information technology that follows quantum communication [7] and quantum computing [8,9], which aims to achieve higher-precision measurements using quantum strategies. Along with the latest technological advances in quantum optics, electricity, and optomechanical vibronic systems, quantum metrology has been applied to many practical tasks, which have significantly boosted the development of related fields, such as gravitational wave detection [10,11], force sensing [12,13], magnetic force measurement [14], clocks [15,16], and biological measurements [17,18].

As fundamental physical quantities, the precision measurement of time and frequency is an essential ingredient of quantum metrology [1,2]. According to these studies, enhancing the detection accuracy of radar becomes an important potential application. Several quantum radar schemes have been proposed, such as quantum illumination [19–24], quantum positioning [15], and three-dimensional accuracy-enhanced quantum radar [25,26], some of which have also been demonstrated in experiments [27,28]. Most of the current research can be attribute to a single parameter estimation problem, such as determining positions or velocities. The ultimate measurement accuracy of them that can be achieved is determined by the quantum Cramér-Rao bound (QCRB) [3,29–31], which is obtained by analyzing the quantum Fisher information (QFI) [3,29–31]. Compared to classical strategies, quantum strategies can improve accuracy and sensitivity, where the maximum accuracy achievable for a single parameter is the Heisenberg limit, which transcends the standard quantum limit. However, in various application scenarios, the positioning of the multibody system, and the size of the object, we actually need to determine different physical quantities simultaneously, such as the simultaneous estimation of the central position and relative velocity. Although quantum multiparameter estimation has started to be explored [29,30], few generalized quantum positioning schemes were designed based on quantum multiparameter estimation theory. With respect to multiparameter estimation, subject to the noncommuting relation between different observables, it often exists as a tradeoff, i.e., Heisenberg's uncertainty principle [32,33]. Zhuang *et al.* proposed entanglement-induced lidar for measuring a target's range and velocity [34]. Recently, Huang *et al.* showed that the tradeoff in simultaneously estimating both time and frequency can be weakened when using entangled states as probe states [35]. In this study we introduce a quantum strategy aimed at simultaneously estimating two distinct physical quantities in various application scenarios utilizing different quantum entanglement resources. Specifically, we investigate the utilization of photons with positive time correlation or negative time correlation.

First, we propose a method for detecting the central position and relative velocity of a multibody system by measuring the time sum and frequency difference. Second, we present a technique for precisely measuring the size and velocity of moving objects. To provide a comprehensive analysis, we delve into the accuracy limits of the aforementioned estimation parameters when employing the quantum illumination strategy and the single-photon strategy mentioned earlier. Our results demonstrate that when appropriate entanglement sources are utilized and the entanglement degree is relatively high, this strategy exhibits a superior quantum advantage compared to the other two strategies.

The article is structured as follows. In Sec. II we delve into the estimation of the central position and relative velocity of two-object systems. We employ quantum multiparameter

*Corresponding author: renchangliang@hunnu.edu.cn

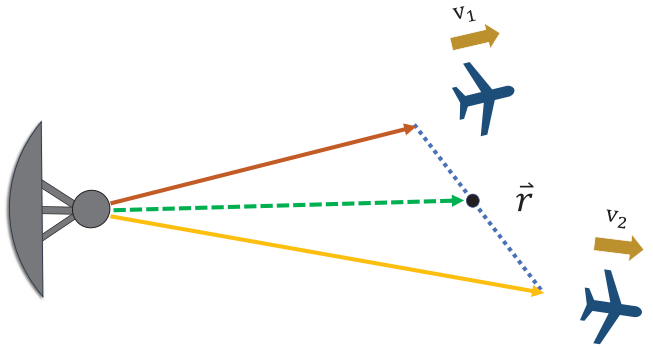

FIG. 1. Illustration of the central position and relative velocity detection in a multibody system.

estimation theory to establish a comprehensive method for analyzing the measurement accuracy limits across different schemes. Section III introduces quantum strategies specifically designed for measuring the size and velocity of objects. We outline approaches employed in this context. Section IV presents the concluding remarks and summarizes the key findings, as well as provides an outlook for future work.

II. ESTIMATION OF GROUP MOTION OF A MULTIBODY SYSTEM

We present a method for detecting the central position and relative velocity of a multibody system through the measurement of the time sum and frequency difference. To describe the concept, let us examine a basic multibody system consisting of two objects as an illustrative example. As illustrated in Fig. 1, supposed that two photons arrive at two objects moving with velocities v_1 and v_2 after travel times $\frac{\bar{t}_1}{2}$ and $\frac{\bar{t}_2}{2}$, respectively. The position $\vec{r}_1 = \vec{c}_1\frac{\bar{t}_1}{2}$ of object A and the position $\vec{r}_2 = \vec{c}_2\frac{\bar{t}_2}{2}$ of object B can be measured. Hence the central position between these two objects can be expressed as

$$\vec{r} = \frac{\vec{c}_1\bar{t}_1 + \vec{c}_2\bar{t}_2}{4}, \tag{1}$$

where $\vec{c}_1$ and $\vec{c}_2$ are two velocity vectors of the returned photons. The two objects are located at a considerable distance from the radar, $\vec{c}_1 \approx \vec{c}_2$, enabling their central position to be precisely determined as $\vec{r} = \frac{\vec{c}(\bar{t}_1+\bar{t}_2)}{4}$. Obviously, the accuracy of determining the central position relies on the variance of $\bar{t}_1 + \bar{t}_2$. In addition, the relative velocity of two objects can also be estimated by the Doppler effect. The relation between the difference in frequency and the difference in velocity can be described as

$$\begin{aligned}\bar{\omega}_2 - \bar{\omega}_1 &= \left(\frac{c - v_2}{c + v_2}\bar{\omega}_0 - \bar{\omega}_0\right) - \left(\frac{c - v_1}{c + v_1}\bar{\omega}_0 - \bar{\omega}_0\right) \\ &\simeq \frac{2(v_2 - v_1)}{c}\bar{\omega}_0,\end{aligned} \tag{2}$$

where $\bar{\omega}_0$ is the central frequency of the initial pulse and $\bar{\omega}_1$ and $\bar{\omega}_2$ are the central frequencies of the returned photons from different directions. Similarly, the accuracy of determining the relative velocity of two objects relies on the variance of $\bar{\omega}_2 - \bar{\omega}_1$.

To accomplish the task, we initially utilize a two-qubit entangled state where two photons are emitted to these two objects respectively. In this context, we are specifically focusing on the ideal scenario where the direction is precisely defined and the photons experience highly efficient reflection. Without loss of generality, the initial emitted state can be described in the time domain

$$|\psi\rangle = \iint \phi_0(t_1, t_2)|t_1\rangle|t_2\rangle dt_1 dt_2, \tag{3}$$

where $|t_i\rangle = \hat{a}^\dagger(t_i)|0\rangle$ is a single-photon state at t_i with $i = 1, 2$, $\hat{a}^\dagger(t_i)$ is the creation operator, and $\phi_0(t_1, t_2)$ is biphoton temporal wave function. We choose $\phi_0(t_1, t_2) = \sqrt{\frac{2\sqrt{1-\kappa^2}\sigma_0^2}{\pi}}e^{-\sigma_0^2(t_1^2+t_2^2-2\kappa t_1 t_2)}e^{-i\bar{\omega}_0(t_1+t_2)}$, where $\bar{\omega}_0$ and σ_0 are the carrier frequency and bandwidth for each single photon. The parameter $\kappa \in (-1, 1)$ quantifies the amount of entanglement between the two photons. As κ approaches 1, the biphoton state is positively correlated in time, whereas when κ approaches -1, the two photons will negatively correlated in time; $\kappa = 0$ means they are separate states.

The two photons of the biphoton state experience backscattering and subsequently exhibit a time delay upon their return (a detailed derivation can be found in [35]; also refer to Appendix B). Without loss of generality, the returned biphoton state can be expressed as

$$|\psi'\rangle = \iint \phi(t_1, t_2)|t_1\rangle|t_2\rangle dt_1 dt_2, \tag{4}$$

where

$$\begin{aligned}\phi(t_1, t_2) = &\sqrt{\frac{2\sqrt{1-\kappa^2}\sigma_1\sigma_2}{\pi}}e^{-i\bar{\omega}_1(t_1-\bar{t}_1)}e^{-i\bar{\omega}_2(t_2-\bar{t}_2)} \\ &\times e^{-\left[(t_1-\bar{t}_1)^2\sigma_1^2+(t_2-\bar{t}_2)^2\sigma_2^2-2\kappa\sigma_1\sigma_2(t_1-\bar{t}_1)(t_2-\bar{t}_2)\right]},\end{aligned}$$

with

$$\begin{aligned}\sigma_i &= \frac{c - v_i}{c + v_i}\sigma_0, \quad \bar{t}_i = \frac{2r_i}{c - v_i}, \\ \bar{\omega}_1 &= \frac{c - v_1}{c + v_1}\bar{\omega}_0, \quad \bar{\omega}_2 = \frac{c - v_2}{c + v_2}\bar{\omega}_0.\end{aligned} \tag{5}$$

As the goal is to compute the QFI matrix for the estimation of the central position and relative velocity, according to Eqs. (1) and (2), it is better to define the variables $\bar{\omega}_- = \bar{\omega}_2 - \bar{\omega}_1$, $\bar{t}_+ = \bar{t}_1 + \bar{t}_2$, $\bar{\omega}_+ = \bar{\omega}_1 + \bar{\omega}_2$, and $\bar{t}_- = \bar{t}_2 - \bar{t}_1$. After performing detailed and coherent calculations (refer to Appendixes B and C 1), we derive a precise expression for the QFI matrix, allowing us to accurately estimate $\bar{t}_+$ and $\bar{\omega}_-$,

$$H(\bar{t}_+, \bar{\omega}_-) = \begin{pmatrix} 2(1-\kappa)\sigma^2 & 0 \\ 0 & \frac{1}{2(1+\kappa)\sigma^2} \end{pmatrix}. \tag{6}$$

According to the necessary and sufficient condition for joint optimal estimation [31], we find $\mathrm{Tr}(\rho[L_{\bar{t}_+}, L_{\bar{\omega}_-}]) = 0$, where L_λ is the symmetric logarithmic derivative matrix. Therefore, by utilizing an entangled photon state that exhibits negatively temporal correlation as the emission source, we can achieve the saturation of the QCRB [3,29–31], indicating that the estimation of the time sum and the frequency difference can be optimally achieved. Obviously, the variance of the estimator $\bar{t}_+$ depends on the reciprocal of $2(1-\kappa)\sigma^2$, while the variance of the estimator $\bar{\omega}_-$ depends on the reciprocal of $\frac{1}{2(1+\kappa)\sigma^2}$. These two terms can be arbitrarily

small simultaneously. The relation of estimating $\bar{t}_+$ and $\bar{\omega}_-$ can be expressed as

$$\delta\bar{t}_+\delta\bar{\omega}_- \geqslant \frac{\sqrt{1+\kappa}}{\sqrt{1-\kappa}}. \tag{7}$$

Clearly, when $\kappa \to -1$, the right-hand side of this relation tends towards zero, indicating that the tradeoff in precision between $\bar{t}_+$ and $\bar{\omega}_-$ can be alleviated. As κ deviates from -1, the accuracy of joint estimation deteriorates progressively. For every value of κ, the lower bound on Eq. (7) can be attained by detecting the returned state through time-resolved photon counting. In fact, the accuracy of joint estimation of $\bar{t}_+$ and $\bar{\omega}_-$ directly influences the accuracy of estimating the central position and the relative velocity. This analysis is conducted directly and discussed in detail in Appendix A. When $\kappa = 0$, the state of the two photons evolves into a product of two single-photon states, and the accuracy of joint estimation of $\bar{t}_+$ and $\bar{\omega}_-$ becomes $\delta\bar{t}_+\delta\bar{\omega}_- \geqslant 1$. Remarkably, even when using a laser, which involves the product of two coherent states rather than the product of two single-photon states, the exact same uncertainty relation can be obtained. We have supplied a rigorous proof in Appendix C 4. The performance of coherent states was also shown in Ref. [36].

Compared with the biphoton state, we can initially utilize two single-photon states as the emitted resource where two photons are emitted to these two objects independently. Each single-photon state can be described as $|\psi_i\rangle = \int \psi_0(t_i)|t_i\rangle dt_i$ initially, where the temporal distribution is $\psi_0(t_i) = (\frac{2\sigma_0^2}{\pi})^{1/4} e^{-t_i^2\sigma_0^2} e^{-i\bar{\omega}t_i}$ with the same spectrum $\phi_0(t_1, t_2)$ as in Eq. (3). These two photons experience backscattering and subsequently exhibit a time delay upon their return. The density matrix of the returned two single-photon states can be described by [35,37]

$$\rho_1 = (|\psi_1\rangle\langle\psi_1| + |\psi_2\rangle\langle\psi_2|), \tag{8}$$

where $|\psi_i\rangle = \int \psi_i(t_i)|t_i\rangle dt_i$ and the temporal distribution is $\psi_i(t_i) = (\frac{2\sigma_i^2}{\pi})^{1/4} e^{-(t_i-\bar{t}_i)^2\sigma_i^2} e^{-i\bar{\omega}_i(t_i-\bar{t}_i)}$. It is important to note that, in order to compare with other strategies using the same photon number, Eq. (8) is not normalized.

As illustrated in Appendix C2, the QFI matrix that allows us to accurately estimate the estimators $\bar{t}_+$ and $\bar{\omega}_-$ is given by

$$H = \begin{pmatrix} H_{\bar{t}_+^2} & 0 \\ 0 & H_{\bar{\omega}_-^2} \end{pmatrix}, \tag{9}$$

where $H_{\bar{t}_+^2} = 2\sigma^2 + \varepsilon_{\bar{t}_+} > 0$, $H_{\bar{\omega}_-^2} = \frac{1}{2\sigma^2} + \varepsilon_{\bar{\omega}_-} > 0$, $\varepsilon_{\bar{t}_+} \leqslant 0$, and $\varepsilon_{\bar{\omega}_-} \leqslant 0$ (see Appendix C2 for detailed expressions of $\varepsilon_{\bar{t}_+}$ and $\varepsilon_{\bar{\omega}_-}$). Clearly, we find $H_{\bar{t}_+^2} \leqslant 2\sigma^2$ and $H_{\bar{\omega}_-^2} \leqslant \frac{1}{2\sigma^2}$. Likewise, the estimation of the time sum and the frequency difference can be achieved optimally because $\mathrm{Tr}(\rho[L_{\bar{t}_+}, L_{\bar{\omega}_-}]) = 0$. Hence, the joint estimation for $\bar{t}_+$ and $\bar{\omega}_-$ satisfies

$$\delta\bar{t}_+\delta\bar{\omega}_- \geqslant 1. \tag{10}$$

Obviously, due to entanglement, the biphoton state can achieve a much lower bound in terms of joint measurement accuracy of the time sum and frequency difference, and this advantage will be lost when $\kappa \geqslant 0$.

Likewise, we can also measure the multibody relative velocity and the central position using the quantum illumination-based scheme, as discussed by Huang *et al.* [35]. To accomplish the task, we need two pairs of entangled photons; the signal photon of each pair will emit to the two objects respectively, while their idler photons remain. By jointly measuring each scattered signal photon and the corresponding idler photon, the distance and velocity of each object can be obtained from the time delay and frequency shift of the scattered signal photon respectively. Hence the relative velocity and central position of this multibody system are estimated by first measuring the distance and velocity information of each object. Therefore, this scheme is actually similar to the single-photon scheme; the density matrix of the used state can be expressed as $\rho_2 = \frac{1}{2}(|\Psi_1\rangle\langle\Psi_1| + |\Psi_2\rangle\langle\Psi_2|)$, where $|\Psi_i\rangle$ is a biphoton entangled state as defined Eq. (4). Unlike the single-photon scheme, the tradeoff in simultaneously estimating both time and frequency can be weakened when one uses entangled states as probe states. Similarly, we can derive the QFI matrix that allows us to accurately estimate the estimators $\bar{t}_+$ and $\bar{\omega}_-$, which is

$$H = \begin{pmatrix} H_{\bar{t}_+^2} & 0 \\ 0 & H_{\bar{\omega}_-^2} \end{pmatrix},$$

where $H_{\bar{t}_+^2} = \sigma^2 + \varepsilon_{\bar{t}_+}$ and $H_{\bar{\omega}_-^2} = \frac{1}{4(1-\kappa^2)\sigma^2} + \varepsilon_{\bar{\omega}_-}$. In this scheme, the joint estimation for $\bar{t}_+$ and $\bar{\omega}_-$ satisfies

$$\delta\bar{t}_+\delta\bar{\omega}_- \geqslant 2\sqrt{1-\kappa^2}. \tag{11}$$

This implies that the uncertainty of simultaneously estimating $\bar{t}_+$ and $\bar{\omega}_-$ can be reduced by a factor $2\sqrt{1-\kappa^2}$ using this scheme.

As depicted in Fig. 2(a), we can compare the estimation accuracy of the central position and relative velocity for various types of detection sources and strategies. To ensure fairness, we maintain consistency by employing an equal number of photons for different probing strategies. The lower bound of the uncertainty of simultaneously estimating $\bar{t}_+$ and $\bar{\omega}_-$, denoted by $\min(\delta\bar{t}_+\delta\bar{\omega}_-)$, is a function of the parameter κ for different strategies. In our strategy, we achieve $\min(\delta\bar{t}_+\delta\bar{\omega}_-) = \frac{\sqrt{1+\kappa}}{\sqrt{1-\kappa}}$ (blue line), while the quantum illumination scheme yields $\min(\delta\bar{t}_+\delta\bar{\omega}_-) = 2\sqrt{1-\kappa^2}$ (green line). In the single-photon strategy, $\min(\delta\bar{t}_+\delta\bar{\omega}_-)$ remains constant at 1 throughout.

It is clearly shown that when utilizing a negatively time-correlated entanglement source for estimation, $\kappa \in (-1, 0)$, our scheme proves to be optimal. However, for a positively time-correlated entanglement source, the situation varies depending on the quality of the entanglement. Our strategy and the quantum illumination strategy fall short of the performance achieved by the single-photon strategy, when the entanglement is relatively weak, $\kappa \in (0, \frac{\sqrt{3}}{2})$. Conversely, when the entanglement source approaches ideal positively correlated in time, $\kappa \in (\frac{\sqrt{3}}{2}, 1)$, the quantum illumination strategy emerges as the optimal solution.

The same analytical strategy can be readily extended to more general scenarios. For instance, in the context of multibody systems, we can estimate both the central position of the entire system and the relative velocity between a fixed

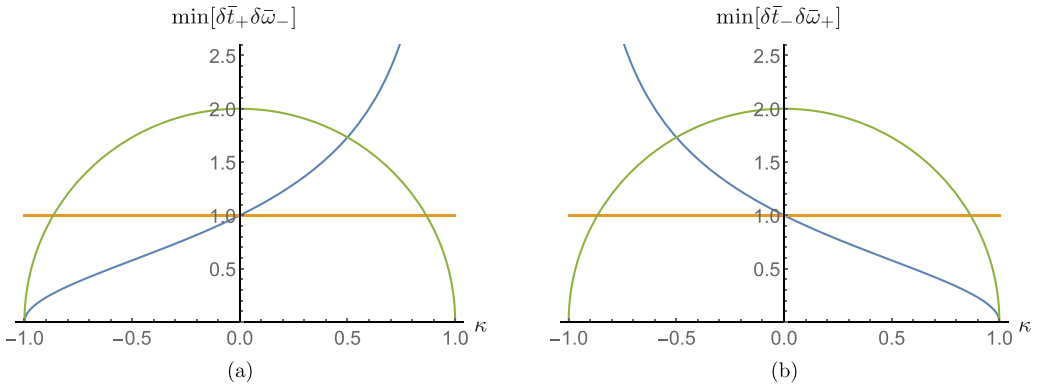

FIG. 2. (a) Accuracy limit of the simultaneous estimation of the time sum and frequency difference for different strategies. (b) Accuracy limit of the simultaneous estimation of the time difference and frequency sum for different strategies. The blue, green, and yellow lines correspond to our strategy, quantum illumination strategy, and single-photon strategy, respectively.

subsystem and the remaining subsystems. Supposed that N photons are emit toward N objects with different positions respectively and arrive at them after travel times $\frac{\bar{t}_1}{2}, \ldots, \frac{\bar{t}_N}{2}$; the central position among these N objects is $\vec{r} = \frac{\vec{r}_1+\cdots+\vec{r}_N}{N} = \frac{\vec{c}_1\bar{t}_1+\cdots+\vec{c}_N\bar{t}_N}{2N}$. The objects are located at a considerable distance from the radar, enabling the central position of N objects to be $\vec{r} = \frac{c(\bar{t}_1+\cdots+\bar{t}_N)}{2N}$. The accuracy of the central position depends on the time sum of N photons. Different probe states result in different detection accuracies. Compared with the N-photon separate state, the N-photon entangled state can achieve a much lower accuracy bound [3,38]. Similarly, the Doppler effect can also be used to estimate the relative velocity between the ith object and the remaining objects. This relation between the difference in frequency and the difference in velocity can be expressed as $\bar{\omega}_i - \frac{\sum_{n=1,n\neq i}^{N-1}\bar{\omega}_n}{N-1} \simeq \frac{2(v_i-\vec{v})}{c}\bar{\omega}_0$, where $\vec{v} = \sum_{n=1,n\neq i}^{N-1} v_n$. The accuracy of determining the relative velocity of two objects relies on the variance of $\bar{\omega}_i - \frac{\sum_{n=1,n\neq i}^{N-1}\bar{\omega}_n}{N-1}$. It is important to stress that this task is the most straightforward among those applicable to multibody systems. In the context of multibody systems, there exists a plethora of more intricate and intriguing tasks deserving of exploration.

III. MEASURING THE RELATIVE SIZE AND VELOCITY OF MOVING OBJECTS

We present a method to precisely measure the size and velocity of moving objects. In our scenario, we focus on measuring a far-field moving target with velocity in the detection direction. The targets have well-defined sizes and radial distributions. We are particularly interested in measuring the relative radial distance between two distinct regions of the target and the velocity of the target. By iteratively performing this procedure, we can achieve comprehensive imaging of the target. As illustrated in Fig. 3, the object moves in the radial direction of the radar with velocity v.

Assuming that the distances between two distinct points on an object, labeled A and B, and the radar are R_0 and $R_0 + x$, respectively, where x represents the relative difference in size between the two points. To accomplish this task, a minimum of two photons is required. When the radar emits two photons simultaneously that are backscattered by the two distinct points of the object respectively, each photon will return with a travel time $\bar{t}_i$ and a central frequency $\bar{\omega}_i$. According to Eq. (5), it is easy to obtain that $\bar{t}_1 = \frac{2R_0}{c-v}$ and $\bar{t}_2 = \frac{2R_0+2x}{c-v}$. Hence the time difference caused by the size of the object is $\bar{t}_2 - \bar{t}_1 = \frac{2x}{c-v} \approx \frac{2x}{c}$, and the distance between the two distinct points can be given as

$$x = \frac{c(\bar{t}_2 - \bar{t}_1)}{2}. \tag{12}$$

Clearly, the accuracy of determining the distance x relies on the variance of $\bar{t}_2 - \bar{t}_1$. Likewise, the velocity of the object can be estimated by analyzing the frequency shift of the returned photons. According to the Doppler effect, the carrier frequency of the returned photons will change as $\bar{\omega}_i = \frac{c-v}{c+v}\bar{\omega}_0$, so the frequency shift determines $\triangle\omega_i = \bar{\omega}_i - \bar{\omega}_0 \approx \frac{2\bar{\omega}_0 v}{c}$. Although it is possible to measure velocity using a single photon, at least two photons are necessary for the complete task, especially for measuring the size of the object. Hence, we analyze the process of employing two photons to measure the velocity of an object. At first glance, this may seem like a trivial process. Assuming that two photon pulses have identical initial central frequencies and the velocity of each part of the object is the same, the frequency shift of the returned photons will satisfy $\triangle\omega_1 = \triangle\omega_2 = \triangle\omega$. The velocity of the object can be estimated by summing up the frequency shifts of the two

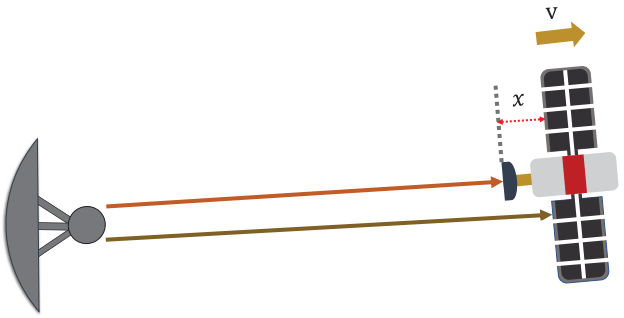

FIG. 3. Illustration showing the measurement of the relative size and velocity of a moving object.

photons, which can be given as

$$v = \frac{c}{2\bar{\omega}_0}(\bar{\omega}_1 + \bar{\omega}_2 - 2\bar{\omega}_0) = \frac{c\triangle\omega}{\bar{\omega}_0}. \tag{13}$$

Hence, the accuracy of determining the velocity relies on the variance of $\bar{\omega}_1 + \bar{\omega}_2$. It is possible to reduce this variance to infinitesimal levels using specialized photon states, thereby enhancing the precision of measuring velocity.

Likewise, employing a two-photon entangled state (3) as the emission source directed towards the object, and subsequently the photons reflected back, the returned biphoton state will change as Eq. (4). After performing detailed and coherent calculations (refer to Appendixes B and D1), we derive a precise expression for the QFI matrix, allowing us to accurately estimate $\bar{t}_-$ and $\bar{\omega}_+$,

$$H(\bar{t}_-, \bar{\omega}_+) = \begin{pmatrix} 2(1+\kappa)\sigma^2 & 0 \\ 0 & \frac{1}{2(1-\kappa)\sigma^2} \end{pmatrix}. \tag{14}$$

We compute the necessary and sufficient condition $\mathrm{Tr}(\rho[L_{\bar{t}_-}, L_{\bar{\omega}_+}]) = 0$, indicating that the parameters $\bar{t}_-$ and $\bar{\omega}_+$ can be optimally estimated jointly. Obviously, the variance of $\bar{t}_-$ depends on the reciprocal of $2(1+\kappa)\sigma^2$, while the variance of $\bar{\omega}_+$ depends on the reciprocal of $\frac{1}{2(1-\kappa)\sigma^2}$. Therefore, we can obtain

$$\delta\bar{t}_-\delta\bar{\omega}_+ \geqslant \frac{\sqrt{1-\kappa}}{\sqrt{1+\kappa}}. \tag{15}$$

Notably, when $\kappa \to 1$, the right-hand side of this relation tends towards zero. As κ deviates from 1, the accuracy of joint estimation deteriorates progressively. For every value of κ, the lower bound on Eq. (15) can be achieved by detecting the returned state through time-resolved photon counting. When $\kappa = 0$, the state of the two photons transforms into a product of two single-photon states. In this case, the accuracy of jointly estimating $\bar{t}_-$ and $\bar{\omega}_+$ yields $\delta\bar{t}_-\delta\bar{\omega}_+ \geqslant 1$. Remarkably, this same uncertainty relation can also be achieved even when a laser is used, which combines two coherent states rather than two single-photon states.

For the probing state being two single-photon states, according to the photon's travel time and frequency shift, the photon state returned can be expressed as Eq. (8). As illustrated in Appendix D 2, the QFI matrix that allows us to accurately estimate $\bar{t}_-$ and $\bar{\omega}_+$ is

$$H = \begin{pmatrix} H_{\bar{t}_-^2} & 0 \\ 0 & H_{\bar{\omega}_+^2} \end{pmatrix}, \tag{16}$$

where $H_{\bar{t}_-^2} = 2\sigma^2 + \varepsilon_{\bar{t}_-} > 0$ and $H_{\bar{\omega}_+^2} = \frac{1}{2\sigma^2} + \varepsilon_{\bar{\omega}_+} > 0$, with $\varepsilon_{\bar{t}_-} \leqslant 0$ and $\varepsilon_{\bar{\omega}_+} \leqslant 0$ (refer to Appendix D 2 for detailed expressions of $\varepsilon_{\bar{t}_-}$ and $\varepsilon_{\bar{\omega}_+}$). Also, we compute the necessary and sufficient condition $\mathrm{Tr}(\rho[L_{\bar{t}_-}, L_{\bar{\omega}_+}]) = 0$. The joint estimation for the time difference and frequency sum is shown as

$$\delta\bar{t}_-\delta\bar{\omega}_+ \geqslant 1. \tag{17}$$

The bound on the estimated time difference and frequency sum of the two single-photon states is much higher than that of the biphoton entangled state, and this advantage will be lost when $\kappa \leqslant 0$. Moreover, we can achieve precise measurements of the size and velocity of the moving target by employing a quantum illumination-based strategy. This approach also requires two pairs of entangled photons. A detailed discussion of the method is provided in the Appendix D 3 for reference. In this scheme, the joint estimation for $\bar{t}_-$ and $\bar{\omega}_+$ satisfies

$$\delta\bar{t}_-\delta\bar{\omega}_+ \geqslant 2\sqrt{1-\kappa^2}. \tag{18}$$

This implies that the uncertainty of simultaneously estimating $\bar{t}_-$ and $\bar{\omega}_+$ can be reduced by a factor $2\sqrt{1-\kappa^2}$.

As depicted in Fig. 2(b), we can compare the estimation accuracy of the size and velocity of moving objects for various types of detection sources and strategies. To ensure fairness, we maintain consistency by employing an equal number of photons for different probing strategies. The lower bound of the uncertainty of simultaneously estimating $\bar{t}_-$ and $\bar{\omega}_+$, denoted by $\min(\delta\bar{t}_-\delta\bar{\omega}_+)$, is a function of the parameter κ for different strategies. In our strategy, we achieve $\min(\delta\bar{t}_-\delta\bar{\omega}_+) = \frac{\sqrt{1-\kappa}}{\sqrt{1+\kappa}}$ (blue line), while the quantum illumination scheme yields $\min(\delta\bar{t}_-\delta\bar{\omega}_+) = 2\sqrt{1-\kappa^2}$ (green line). In the single-photon strategy, $\min(\delta\bar{t}_-\delta\bar{\omega}_+)$ remains constant at 1 throughout.

It is clearly shown that, when utilizing a positively time-correlated entanglement source for estimation, $\kappa \in (0, 1)$, our scheme proves to be optimal. However, for a negatively time-correlated entanglement source, the situation varies depending on the quality of the entanglement. Our strategy and the quantum illumination strategy fall short of the performance achieved by the single-photon strategy, when the entanglement is relatively weak, $\kappa \in (-\frac{\sqrt{3}}{2}, 0)$. Conversely, when the entanglement source approaches ideal negatively correlated in time, $\kappa \in (-1, -\frac{\sqrt{3}}{2})$, the quantum illumination strategy similarly emerges as the optimal solution.

IV. CONCLUSION

We have presented a quantum strategy for simultaneous estimation of two distinct physical quantities in various application scenarios, utilizing different quantum entanglement resources. Specifically, we explored the utilization of photons with positive or negative time correlation.

The first aspect of our work focused on proposing a method for detecting the central position and relative velocity of a multibody system through the measurement of time sum and frequency difference. Additionally, we presented a technique for precise measurement of the size and velocity of moving objects.

To provide a comprehensive analysis, we investigated the accuracy limits of the estimation parameters mentioned above, comparing them with the quantum illumination strategy and the single-photon strategy discussed earlier. Notably, our results highlight that when appropriate entanglement sources are utilized and the entanglement degree is relatively high, the proposed quantum strategy exhibits a superior quantum advantage over the other two strategies.

Overall, this study sheds light on the potential of leveraging quantum entanglement in simultaneous estimation tasks, demonstrating its superiority under certain conditions. These findings contribute to advancing our understanding of quantum strategies for accurate measurements in diverse scenarios.

As a prospective application, it is both intriguing and significant to extend the discussion to the three-dimensional case

with robustness against noise. For this extension, we can draw insights from recent work using Gaussian entangled sources to enable three-dimensional positioning [39]. In this context, we can take into consideration the longitudinal and transverse transmission of light during propagation, bringing us closer to a practical scenario. The use of specialized entanglement sources, such as those with positive correlations in time and momentum [40,41], can lead to higher-precision spatial measurements [25]. In addition, previous work [25] also provides valuable insights for addressing the three-dimensional situation. Regarding noise resistance, several strategies [42–44] have been proposed to reduce its impact, albeit at the cost of resolution. For instance, partially entangled states exhibit more resilience to photon loss, retaining some information about the object's position. Furthermore, exploring alternative sources for suitable compression is worth discussing [45]. Recent approaches involving the utilization of random coherent states also warrant further investigation [46]. The exploration of these topics is left for future research.

ACKNOWLEDGMENTS

We appreciate Lorenzo Maccone for his valuable comments and discussions. C.R. was supported by the National Natural Science Foundation of China (Grants No. 12075245 and No. 12247105), the Natural Science Foundation of Hunan Province (Grant No. 2021JJ10033), Xiaoxiang Scholars Programme of Hunan Normal University, and Hunan provincial major sci-tech program No. (2023zk1010).

APPENDIX A: QUANTUM FISHER INFORMATION

We review the basic concepts of quantum Fisher information. In many cases, the estimation of certain physical parameters relies on the association with another covariate. For example, the position of a target can be estimated based on the travel time of single photons. In the context of unbiased estimators, the QCRB determines the precision of the parameter estimation

$$\delta\lambda^2 \geqslant \frac{1}{NH}, \tag{A1}$$

where λ represents the estimated parameter, H denotes the QFI matrix, and N corresponds to the number of measurements. The QFI matrix is given by

$$H = \tfrac{1}{2}\mathrm{Tr}\big[\rho\big(L_{\lambda_i}L_{\lambda_j} + L_{\lambda_j}L_{\lambda_i}\big)\big], \tag{A2}$$

where $\rho = \sum \rho_{ij}|e_i\rangle\langle e_j|$ is the density matrix of the state expanded in an orthogonal basis and L_{λ_i} and L_{λ_j} are the symmetric logarithmic derivative (SLD) matrices [31]. The SLD matrix can be given as

$$L_{\lambda_{ij}} = 2\frac{\langle e_i|\partial_\lambda\rho|e_j\rangle}{\rho_{ii}+\rho_{jj}}, \tag{A3}$$

where ρ_{ii} and ρ_{jj} are the elements of the density matrix and $L_{\lambda_{ij}}$ is the element of the SLD matrix. If the joint estimation of multiparameters is considered, a necessary and sufficient condition for the joint and optimal estimation is that the SLD operators commute, i.e.,

$$\mathrm{Tr}\big(\rho\big[L_{\lambda_i}, L_{\lambda_j}\big]\big) = 0. \tag{A4}$$

If the estimated parameter is not the expected parameter, the correspondence between the covariate and parameter can be given as

$$L_{\bar{\gamma}} = 2\frac{\langle e_i|\frac{\partial\rho}{\partial\bar{\lambda}}\frac{\partial\bar{\lambda}}{\partial\bar{\gamma}}|e_j\rangle}{\rho_{ii}+\rho_{jj}}, \tag{A5}$$

where $\bar{\gamma}$ and $\bar{\lambda}$ are the actual estimated parameter and the covariate, respectively. In this discussion, we use time and frequency to estimate distance and velocity, respectively. The partial derivatives are

$$\frac{\partial\bar{t}}{\partial r} = \frac{2}{c(1-\Gamma)}, \quad \frac{\partial\bar{t}}{\partial\Gamma} = \frac{2r}{(1-\Gamma)^2},$$
$$\frac{\partial\bar{\omega}}{\partial r} = 0, \quad \frac{\partial\bar{\omega}}{\partial\Gamma} = -\frac{2\bar{\omega}_0}{(1-\Gamma)^2}, \tag{A6}$$

with $\Gamma = \frac{v}{c}$, which has been given in [35]. The SLD matrix of the velocity and position and the QFI matrix can be written in correspondence to the above.

APPENDIX B: REFLECTED PHOTON STATE IN THE TIME DOMAIN

Assuming that the distance between the moving target and the radar at time $t_0 = 0$ is r and the photon emitted at time t is reflected by the target, the photon will return at the time

$$\tau = t + \frac{2r+2vt}{c-v} = t + \frac{2r}{c-v} + \frac{2vt}{c-v}, \tag{B1}$$

where v is the velocity of the moving target. Due to the Doppler effect, the frequency will change as

$$\bar{\omega} = \frac{c-v}{c+v}\bar{\omega}_0, \tag{B2}$$

where $\bar{\omega}$ is the carrier frequency of returned photons.

If two moving targets with radial velocities are v_1 and v_2, respectively, we assume that the two photons encountered the two targets and returned to the radar. The two photons emitted at t_1 and t_2 will return to the radar at $\tau_i = t_i + \frac{2r_i}{c-v_i} + \frac{2v_it_i}{c-v_i}$, with $i = 1, 2$. Without loss of generality, the returned photons are described by the state

$$|\psi'\rangle = \iint \phi(\tau_1,\tau_2)|\tau_1\rangle|\tau_2\rangle d\tau_1 d\tau_2. \tag{B3}$$

Combining Eqs. (B1)–(B3), we obtain Eq. (4) in the main text.

The calculation for two independent single-photon states is similar. If the two photons are backscattered by the targets, they will return with a time delay given by Eq. (B1). However, since the scattering source is incoherent, the returned two-photon state is a mixed state as defined in Eq. (8).

APPENDIX C: ESTIMATES OF THE CENTRAL POSITION AND RELATIVE VELOCITY OF THE MULTIBODY SYSTEM

1. Our strategy

The returned biphoton entangled state is Eq. (4). To obtain the QFI matrix, we first derive the orthogonal basis

$$|e_n\rangle = \int e_n(t_+,t_-)|t_+\rangle|t_-\rangle dt_+ dt_-, \tag{C1}$$

where $n = 1, 2, 3$, and the temporal distribution can be expressed as

$$\begin{aligned} e_1(t_+, t_-) &= \phi, \\ e_2(t_+, t_-) &= 2\sqrt{\frac{1}{\sigma_1^2 + \sigma_2^2 - 2\kappa\sigma_1\sigma_2}} \\ &\quad \times [(t_+ + t_- - \bar{t}_+ - \bar{t}_-)\sigma_1^2 - 2\kappa\sigma_1\sigma_2(t_+ - \bar{t}_+) \\ &\quad + \sigma_2^2(t_+ - t_- - \bar{t}_+ + \bar{t}_-)]\phi, \\ e_3(t_+, t_-) &= 2\sqrt{\frac{(1-\kappa^2)\sigma_1^2\sigma_2^2}{\sigma_1^2 + \sigma_2^2 + 2\kappa\sigma_1\sigma_2}}(t_- - \bar{t}_-)\phi. \end{aligned} \tag{C2}$$

Second, the SLD matrices for the estimation of the time sum $\bar{t}_+$ and frequency difference $\bar{\omega}_-$ can be derived,

$$L_{\bar{t}_+} = \begin{pmatrix} 0 & \sqrt{\sigma_1^2 + \sigma_2^2 - 2\kappa\sigma_1\sigma_2} & 0 \\ \sqrt{\sigma_1^2 + \sigma_2^2 - 2\kappa\sigma_1\sigma_2} & 0 & 0 \\ 0 & 0 & 0 \end{pmatrix}$$

and

$$L_{\bar{\omega}_-} = \begin{pmatrix} 0 & 0 & -\frac{i}{2}\sqrt{\frac{\sigma_1^2 - 2\kappa\sigma_1\sigma_2 + \sigma_2^2}{(1-\kappa^2)\sigma_1^2\sigma_2^2}} \\ 0 & 0 & 0 \\ \frac{i}{2}\sqrt{\frac{\sigma_1^2 - 2\kappa\sigma_1\sigma_2 + \sigma_2^2}{(1-\kappa^2)\sigma_1^2\sigma_2^2}} & 0 & 0 \end{pmatrix}. \tag{C3}$$

Therefore, the QFI matrix is

$$H(\bar{t}_+, \bar{\omega}_-) = \begin{pmatrix} \sigma_1^2 - 2\kappa\sigma_1\sigma_2 + \sigma_2^2 & 0 \\ 0 & \frac{\sigma_1^2 - 2\kappa\sigma_1\sigma_2 + \sigma_2^2}{4(1-\kappa^2)\sigma_1^2\sigma_2^2} \end{pmatrix}. \tag{C4}$$

Finally, we obtain the relation

$$\delta\bar{t}_+\delta\bar{\omega}_- \geqslant \sqrt{\frac{1}{H_{\bar{t}_+}H_{\bar{\omega}_-}}} = \frac{2\sqrt{1-\kappa^2}\sigma_1\sigma_2}{\sigma_1^2 - 2\kappa\sigma_1\sigma_2 + \sigma_2^2}. \tag{C5}$$

As $\sigma_1 \approx \sigma_2$, the relation is approximately $\delta\bar{t}_+\delta\bar{\omega}_- \geqslant \sqrt{\frac{1+\kappa}{1-\kappa}}$.

2. Single-photon strategy

For two single-photon states, the returned photons are incoherent and can be described by Eq. (9). The orthogonal basis $|e_n\rangle$ can be derived as

$$\begin{aligned} |e_1\rangle &= \sqrt{\frac{1}{c_1}}(|\psi_1\rangle + e^{i(\bar{t}_-\bar{\omega}_+)/2}|\psi_2\rangle), \\ |e_2\rangle &= \sqrt{\frac{1}{c_2}}(|\psi_1\rangle - e^{i(\bar{t}_-\bar{\omega}_+)/2}|\psi_2\rangle), \\ |e_3\rangle &= \sqrt{\frac{1}{c_3}}(|\partial_{\bar{t}_-}e_1\rangle - \langle e_1|\partial_{\bar{t}_-}e_1\rangle|e_1\rangle), \\ |e_4\rangle &= \sqrt{\frac{1}{c_4}}(|\partial_{\bar{t}_-}e_2\rangle - \langle e_2|\partial_{\bar{t}_-}e_2\rangle|e_2\rangle), \end{aligned} \tag{C6}$$

where c_1, c_2, c_3, and c_4 are normalization factors. The mixed state (8) can be expressed in the orthogonal basis as

$$\rho_1 = C_1(|e_1\rangle\langle e_1| + C_2|e_2\rangle\langle e_2|), \tag{C7}$$

with

$$C_1 = \left(1 + \frac{\sqrt{2\sigma_1\sigma_2}\exp\left(\frac{-\bar{\omega}_-^2 - 4\bar{t}_-^2\sigma_1^2\sigma_2^2}{4(\sigma_1^2+\sigma_2^2)}\right)}{\sqrt{\sigma_1^2+\sigma_2^2}}\right)$$

and

$$C_2 = \left(1 - \frac{\sqrt{2\sigma_1\sigma_2}\exp\left(\frac{-\bar{\omega}_-^2 - 4\bar{t}_-^2\sigma_1^2\sigma_2^2}{4(\sigma_1^2+\sigma_2^2)}\right)}{\sqrt{\sigma_1^2+\sigma_2^2}}\right).$$

According to Eq. (A3), we can obtain that

$$L_{\bar{t}_+} = \begin{pmatrix} 0 & 2a_{12} & 0 & 2a_{14} \\ 2a_{21} & 0 & 2a_{23} & 0 \\ 0 & 2a_{32} & 0 & 0 \\ 2a_{41} & 0 & 0 & 0 \end{pmatrix}, \tag{C8}$$

with $a_{21}^* = a_{12} = C_1\langle\partial_{\bar{t}_+}e_1|e_2\rangle + C_2\langle\partial_{\bar{t}_+}e_2|e_1\rangle$, $a_{41}^* = a_{14} = \langle\partial_{\bar{t}_+}e_1|e_4\rangle$, and $a_{32}^* = a_{23} = \langle\partial_{\bar{t}_+}e_2|e_3\rangle$. Similarly,

$$L_{\bar{\omega}_-} = \begin{pmatrix} a_{11} & 0 & 2a_{13} & 0 \\ 0 & a_{22} & 0 & 2a_{24} \\ 2a_{31} & 0 & 0 & 0 \\ 0 & 2a_{42} & 0 & 0 \end{pmatrix}, \tag{C9}$$

with $a_{11} = \frac{\partial_{\bar{\omega}_-}C_1}{C_1}$, $a_{31}^* = a_{13} = \langle\partial_{\bar{\omega}_-}e_1|e_3\rangle$, $a_{22} = \frac{\partial_{\bar{\omega}_-}C_2}{C_2}$, and $a_{42}^* = a_{24} = \langle\partial_{\bar{\omega}_-}e_2|e_4\rangle$. So the QFI matrix is

$$H = \begin{pmatrix} H_{\bar{t}_+^2} & 0 \\ 0 & H_{\bar{\omega}_-^2} \end{pmatrix}, \tag{C10}$$

where $H_{\bar{t}_+^2} = \sigma_1^2 + \sigma_2^2 + \varepsilon_{\bar{t}_+}$ and $H_{\bar{\omega}^2} = \frac{\sigma_1^2+\sigma_2^2}{4\sigma_1^2\sigma_2^2} + \varepsilon_{\bar{\omega}_-}$, with $\varepsilon_{\bar{t}_+} \leqslant 0$ and $\varepsilon_{\bar{\omega}_-} \leqslant 0$. We calculated the necessary and sufficient condition for joint optimal estimation, $\mathrm{Tr}(\rho[L_{\bar{t}_+}, L_{\bar{\omega}_-}]) = 0$. As $\sigma_1 \approx \sigma_2$, we can determine that

$$\begin{aligned} H_{\bar{t}_+^2} &= 2\sigma^2 - 2\exp\left(-\frac{\bar{\omega}_-^2 + 4\bar{t}_-^2\sigma^4}{4\sigma^2}\right)\bar{t}_-^2\sigma^4, \\ H_{\bar{\omega}_-^2} &= \frac{1}{2\sigma^2} - \frac{\bar{t}_-^2}{2}\left[-1 + \exp\left(\frac{\bar{\omega}_-^2 + 4\bar{t}_-^2\sigma^4}{4\sigma^2}\right)\right]^{-1}. \end{aligned}$$

The relation between $\bar{t}_+$ and $\bar{\omega}_-$ is

$$\delta\bar{t}_+\delta\bar{\omega}_- \geqslant 1. \tag{C11}$$

3. Quantum illumination strategy

For the quantum illumination strategy, the returned state can be described as

$$\rho_2 = \tfrac{1}{2}(|\Psi_1\rangle\langle\Psi_1| + |\Psi_2\rangle\langle\Psi_2|), \tag{C12}$$

where $|\Psi_i\rangle$ is defined in Eq. (5). The orthonormal basis is [35]

$$
\begin{aligned}
|e_1\rangle &= \sqrt{\frac{1}{c_1}}(|\psi_1\rangle + e^{i(\bar{t}_-\bar{\omega}_+)/2}|\psi_2\rangle),\\
|e_2\rangle &= \sqrt{\frac{1}{c_2}}(|\psi_1\rangle - e^{i(\bar{t}_-\bar{\omega}_+)/2}|\psi_2\rangle),\\
|e_3\rangle &= \sqrt{\frac{1}{c_3}}(|\partial_{\bar{t}_-}e_1\rangle - \langle e_1|\partial_{\bar{t}_-}e_1\rangle|e_1\rangle),\\
|e_4\rangle &= \sqrt{\frac{1}{c_4}}(|\partial_{\bar{t}_-}e_2\rangle - \langle e_2|\partial_{\bar{t}_-}e_2\rangle|e_2\rangle),\\
|e_5\rangle &= \sqrt{\frac{1}{c_5}}(|\partial_{\bar{\omega}_-}e_1\rangle\\
&\quad - \langle e_1|\partial_{\bar{\omega}_-}e_1\rangle|e_1\rangle - \langle e_3|\partial_{\bar{\omega}_-}e_1\rangle|e_3\rangle),\\
|e_6\rangle &= \sqrt{\frac{1}{c_6}}(|\partial_{\bar{\omega}_-}e_2\rangle\\
&\quad - \langle e_2|\partial_{\bar{\omega}_-}e_2\rangle|e_2\rangle - \langle e_4|\partial_{\bar{\omega}_-}e_2\rangle|e_4\rangle),
\end{aligned}
\tag{C13}
$$

where c_1, c_2, c_3, c_4, c_5, and c_6 are normalization factors. So the state can be diagonalized as

$$\rho_2 = C_1(|e_1\rangle\langle e_1| + C_2|e_2\rangle\langle e_2|), \tag{C14}$$

with

$$
\begin{aligned}
C_1 &= \left[1 + \exp\left(\frac{-\bar{\omega}_-^2 - 4(1-\kappa^2)\bar{t}_-^2\sigma^4}{8(1-\kappa^2)\sigma^2}\right)\right],\\
C_2 &= \left[1 - \exp\left(\frac{-\bar{\omega}_-^2 - 4(1-\kappa^2)\bar{t}_-^2\sigma^4}{8(1-\kappa^2)\sigma^2}\right)\right].
\end{aligned}
$$

The SLD matrices for $\bar{t}_+$ and $\bar{\omega}_-$ are

$$
L_{\bar{t}_+} = 2\begin{pmatrix}
0 & a_{12} & 0 & a_{14} & 0 & 0\\
a_{21} & 0 & a_{23} & 0 & 0 & 0\\
0 & a_{32} & 0 & 0 & 0 & 0\\
a_{41} & 0 & 0 & 0 & 0 & 0\\
0 & 0 & 0 & 0 & 0 & 0\\
0 & 0 & 0 & 0 & 0 & 0
\end{pmatrix}, \tag{C15}
$$

with $a_{21}^* = a_{12} = C_1\langle\partial_{\bar{t}_+}e_1|e_2\rangle + C_2\langle\partial_{\bar{t}_+}e_2|e_1\rangle$, $a_{41}^* = a_{14} = \langle\partial_{\bar{t}_+}e_1|e_4\rangle$, and $a_{32}^* = a_{23} = \langle\partial_{\bar{t}_+}e_2|e_3\rangle$, and

$$
L_{\bar{\omega}_-} = \begin{pmatrix}
a_{11} & 0 & 2a_{13} & 0 & 2a_{15} & 0\\
0 & a_{22} & 0 & 2a_{24} & 0 & 2a_{26}\\
2a_{31} & & 0 & 0 & 0 & 0\\
0 & 2a_{42} & 0 & 0 & 0 & 0\\
2a_{51} & 0 & 0 & 0 & 0 & 0\\
0 & 2a_{62} & 0 & 0 & 0 & 0
\end{pmatrix}, \tag{C16}
$$

with $a_{11} = \frac{\partial_{\bar{\omega}_-}C_1}{C_1}$, $a_{31}^* = a_{13} = \langle\partial_{\bar{\omega}_-}e_1|e_3\rangle$, $a_{22} = \frac{\partial_{\bar{\omega}_-}C_2}{C_2}$, $a_{42}^* = a_{24} = \langle\partial_{\bar{\omega}_-}e_2|e_4\rangle$, $a_{51}^* = a_{15} = \langle\partial_{\bar{\omega}_-}e_1|e_5\rangle$, and $a_{62}^* = a_{26} = \langle\partial_{\bar{\omega}_-}e_2|e_6\rangle$. The QFI matrix is

$$
H = \begin{pmatrix} H_{\bar{t}_+^2} & 0\\ 0 & H_{\bar{\omega}_-^2}\end{pmatrix}, \tag{C17}
$$

where $H_{\bar{t}_+^2} = \sigma^2 + \varepsilon_{\bar{t}_+}$ and $H_{\bar{\omega}_-^2} = \frac{1}{4(1-\kappa^2)\sigma^2} + \varepsilon_{\bar{\omega}_-}$, with $\varepsilon_{\bar{t}_+} \leqslant 0$ and $\varepsilon_{\bar{\omega}_-} \leqslant 0$, and

$$
\begin{aligned}
\varepsilon_{\bar{t}_+} &= -\exp\left(-\frac{\bar{\omega}_-^2 + 4(1-\kappa^2)\bar{t}_-^2\sigma^4}{4(1-\kappa^2)\sigma^2}\right)\bar{t}_-^2\sigma^4,\\
\varepsilon_{\bar{\omega}_-} &= -\frac{\bar{t}_-^2}{4}\left[-1 + \exp\left(\frac{\bar{\omega}_-^2}{4(1-\kappa^2)\sigma^2} + \bar{t}_-^2\sigma^2\right)\right]^{-1}.
\end{aligned}
$$

Finally, we can obtain the relation

$$\delta\bar{t}_+\delta\bar{\omega}_- \geqslant 2\sqrt{1-\kappa^2}. \tag{C18}$$

4. Performance of our strategy using two separate coherent states

We evaluated the performance using laser light. We employed two coherent states with an average photon number of 1 as the emitted resource, which can be described as

$$|\psi\rangle = |\alpha_1\rangle|\alpha_2\rangle, \tag{C19}$$

where $|\alpha_i\rangle = \sum e^{-|\alpha_i(t_i)|^2/2}\frac{\alpha_i(t_i)^n}{n!}\hat{a}^\dagger(t_i)^n|0\rangle$, and $\alpha_i(t_i)$ has time distribution $\phi_0(t_i)$, where $\phi_0(t_i) = (\frac{2\sigma_0^2}{\pi})^{1/4}e^{-t_i^2\sigma_0^2}e^{-i\bar{\omega}t_i}$. These two states experience backscattering and subsequently exhibit a time delay upon their return. The returned states can be described by

$$|\psi'\rangle = |\alpha_1'\rangle|\alpha_2'\rangle, \tag{C20}$$

where $\alpha_i'(t_i)$ has time distribution $\phi(t_i)$, with $\phi(t_i) = (\frac{2\sigma_i^2}{\pi})^{1/4}e^{-(t_i-\bar{t}_i)^2\sigma_i^2}e^{-i\bar{\omega}_i(t_i-\bar{t}_i)}$.

As we know, the quantum Fisher information satisfies $H(\rho_1\otimes\rho_2) = H(\rho_1) + H(\rho_2)$ for product states. We can derive the QFI matrix for each ρ_i, where $\rho_i = |\alpha_i\rangle\langle\alpha_i|$. Taking ρ_1 as an example, the orthogonal basis for ρ_1 can be described as

$$
\begin{aligned}
|e_1\rangle &= |\alpha_1\rangle,\\
|e_2\rangle &= \left(t_1 - \frac{\bar{t}_+ - \bar{t}_-}{2}\right)\sigma\int dt_1(\alpha_1\hat{a}^+ - \alpha_1^*\hat{a})|\alpha_1\rangle.
\end{aligned}
$$

After calculation, we can obtain the SLD matrices

$$
L_{\bar{t}_+} = \begin{pmatrix} 0 & \sigma\\ \sigma & 0\end{pmatrix} \tag{C21}
$$

and

$$
L_{\bar{\omega}_-} = \begin{pmatrix} 0 & \frac{-i}{2\sigma}\\ \frac{i}{2\sigma} & 0\end{pmatrix}. \tag{C22}
$$

Hence, the QFI matrix for ρ_1 is

$$
H(\bar{t}_+, \bar{\omega}_-) = \begin{pmatrix} \sigma^2 & 0\\ 0 & \frac{1}{4\sigma^2}\end{pmatrix}. \tag{C23}
$$

Similarly, we can give the QFI matrix for ρ_2,

$$
H(\bar{t}_+, \bar{\omega}_-) = \begin{pmatrix} \sigma^2 & 0\\ 0 & \frac{1}{4\sigma^2}\end{pmatrix}. \tag{C24}
$$

Therefore, the total QFI matrix can be expressed as

$$
H(\bar{t}_+, \bar{\omega}_-) = \begin{pmatrix} 2\sigma^2 & 0\\ 0 & \frac{1}{2\sigma^2}\end{pmatrix}. \tag{C25}
$$

Finally, we can obtain the relation

$$\delta\bar{t}_+\delta\bar{\omega}_- \geqslant 1. \tag{C26}$$

This indicates that, even when employing a laser, which entails the combination of two coherent states rather than two single-photon states, the exact same uncertainty relation remains achievable.

APPENDIX D: MEASURING THE SIZE AND VELOCITY OF MOVING TARGETS

1. Our strategy

The biphoton state obtained by the radar is Eq. (5). We estimate two parameters $\bar{t}_-$ and $\bar{\omega}_+$ by QFI. The orthonormal basis can be given by

$$|e_n\rangle = \int e_n(t_+,t_-)|t_+\rangle|t_-\rangle dt_+dt_-, \tag{D1}$$

where $n = 1, 2, 3$ and the spectral distribution functions are

$$\begin{aligned} e_1(t_+,t_-) &= \phi, \\ e_2(t_+,t_-) &= \sqrt{2(1-\kappa)}\sigma(t_+ - \bar{t}_+)\phi, \\ e_3(t_+,t_-) &= \sqrt{2(1+\kappa)}\sigma(t_- - \bar{t}_-)\phi. \end{aligned} \tag{D2}$$

The SLD matrices are

$$L_{\bar{t}_-} = \begin{pmatrix} 0 & \sqrt{2(1+\kappa)}\sigma & 0 \\ \sqrt{2(1+\kappa)}\sigma & 0 & 0 \\ 0 & 0 & 0 \end{pmatrix} \tag{D3}$$

and

$$L_{\bar{\omega}_+} = \begin{pmatrix} 0 & 0 & \frac{-i}{2\sqrt{1-\kappa}\sigma} \\ 0 & 0 & 0 \\ \frac{i}{\sqrt{2(1-\kappa)}\sigma} & 0 & 0 \end{pmatrix}. \tag{D4}$$

The QFI matrix is

$$H(\bar{t}_-,\bar{\omega}_+) = \begin{pmatrix} 2(1+\kappa)\sigma^2 & 0 \\ 0 & \frac{1}{2(1-\kappa)\sigma^2} \end{pmatrix}. \tag{D5}$$

Therefore,

$$\delta\bar{t}_-\delta\bar{\omega}_+ \geqslant \sqrt{\frac{1-\kappa}{1+\kappa}}. \tag{D6}$$

2. Single-photon strategy

For two single-photon states, similarly, the returned state and the basis vectors used to derive the QFI refer to Eqs. (C6) and (C7). The SLD matrices for $\bar{t}_-$ and $\bar{\omega}_+$ are

$$L_{\bar{t}_-} = \begin{pmatrix} a_{11} & 0 & 2a_{13} & 0 \\ 0 & a_{22} & 0 & 2a_{24} \\ 2a_{31} & 0 & 0 & 0 \\ 0 & 2a_{42} & 0 & 0 \end{pmatrix},$$

with $a_{11} = \frac{\partial_{\bar{t}_-}C_1}{C_1}$, $a_{31}^* = a_{13} = \langle\partial_{\bar{t}_-}e_1|e_3\rangle$, $a_{22} = \frac{\partial_{\bar{t}_-}C_2}{C_2}$, and $a_{42}^* = a_{24} = \langle\partial_{\bar{t}_-}e_2|e_4\rangle$, and

$$L_{\bar{\omega}_+} = \begin{pmatrix} 0 & 2a_{12} & 0 & 2a_{14} \\ 2a_{21} & 0 & 2a_{23} & 0 \\ 0 & 2a_{32} & 0 & 0 \\ 2a_{41} & 0 & 0 & 0 \end{pmatrix}, \tag{D7}$$

with $a_{21}^* = a_{12} = C_1\langle\partial_{\bar{\omega}_+}e_1|e_2\rangle + C_2\langle\partial_{\bar{\omega}_+}e_2|e_1\rangle$, $a_{41}^* = a_{14} = \langle\partial_{\bar{\omega}_+}e_1|e_4\rangle$, and $a_{32}^* = a_{23} = \langle\partial_{\bar{\omega}_+}e_2|e_3\rangle$. Then we can obtain the QFI matrix

$$H = \begin{pmatrix} H_{\bar{t}_-^2} & 0 \\ 0 & H_{\bar{\omega}_+^2} \end{pmatrix}, \tag{D8}$$

with $H_{\bar{t}_-^2} = 2\sigma^2 - \frac{\bar{\omega}_-^2}{2}(-1 + e^{(\bar{\omega}_-^2+4\bar{t}_-^2\sigma^4)/4\sigma^2})^{-1}$ and $H_{\bar{\omega}_+^2} = \frac{1}{2\sigma^2} - e^{-(\bar{\omega}_-^2+4\bar{t}_-^2\sigma^4)/4\sigma^2}\frac{\bar{\omega}_-^2}{8\sigma^4}$. With the condition $\mathrm{Tr}(\rho[L_{\bar{t}_-}, L_{\bar{\omega}_+}]) = 0$, the relation of $\bar{t}_-$ and $\bar{\omega}_+$ is

$$\delta\bar{t}_-\delta\bar{\omega}_+ \geqslant 1. \tag{D9}$$

3. Quantum illumination strategy

For the quantum illumination strategy, the returned state and the basis vectors used to derive the QFI refer to Eqs. (C13) and (C14). The SLD matrices for $\bar{t}_-$ and $\bar{\omega}_+$ are

$$L_{\bar{t}_-} = \begin{pmatrix} a_{11} & 0 & 2a_{13} & 0 & 0 & 0 \\ 0 & a_{22} & 0 & 2a_{24} & 0 & 0 \\ 2a_{31} & & 0 & 0 & 0 & 0 \\ 0 & 2a_{42} & 0 & 0 & 0 & 0 \\ 0 & 0 & 0 & 0 & 0 & 0 \\ 0 & 0 & 0 & 0 & 0 & 0 \end{pmatrix}, \tag{D10}$$

with $a_{11} = \frac{\partial_{\bar{t}_-}C_1}{C_1}$, $a_{31}^* = a_{13} = \langle\partial_{\bar{t}_-}e_1|e_3\rangle$, $a_{22} = \frac{\partial_{\bar{t}_-}C_2}{C_2}$, and $a_{42}^* = a_{24} = \langle\partial_{\bar{t}_-}e_2|e_4\rangle$, and

$$L_{\bar{\omega}_+} = 2\begin{pmatrix} 0 & a_{12} & 0 & a_{14} & 0 & a_{16} \\ a_{21} & 0 & a_{23} & 0 & a_{25} & 0 \\ 0 & a_{32} & 0 & 0 & 0 & 0 \\ a_{41} & 0 & 0 & 0 & 0 & 0 \\ 0 & a_{52} & 0 & 0 & 0 & 0 \\ a_{61} & 0 & 0 & 0 & 0 & 0 \end{pmatrix}, \tag{D11}$$

with $a_{21}^* = a_{12} = C_1\langle\partial_{\bar{\omega}_+}e_1|e_2\rangle + C_2\langle\partial_{\bar{\omega}_+}e_2|e_1\rangle$, $a_{41}^* = a_{14} = \langle\partial_{\bar{\omega}_+}e_1|e_4\rangle$, $a_{61}^* = a_{16} = \langle\partial_{\bar{\omega}_+}e_1|e_6\rangle$, $a_{32}^* = a_{23} = \langle\partial_{\bar{\omega}_+}e_2|e_3\rangle$, and $a_{52}^* = a_{25} = \langle\partial_{\bar{\omega}_+}e_2|e_5\rangle$. The QFI matrix is

$$H = \begin{pmatrix} H_{\bar{t}_-^2} & 0 \\ 0 & H_{\bar{\omega}_+^2} \end{pmatrix}, \tag{D12}$$

where $H_{\bar{t}_-^2} = \sigma^2 + \varepsilon_{\bar{t}_-}$ and $H_{\bar{\omega}_+^2} = \frac{1}{4(1-\kappa^2)\sigma^2} + \varepsilon_{\bar{\omega}_+}$, with $\varepsilon_{\bar{t}_-} \leqslant 0$, $\varepsilon_{\bar{\omega}_+} \leqslant 0$, $\varepsilon_{\bar{t}_-} = -(e^{\bar{\omega}_-^2/4(1-\kappa^2)\sigma^2+\bar{t}_-^2\sigma^2} - 1)^{-1}\frac{\bar{\omega}_-^2}{4}$, and $\varepsilon_{\bar{\omega}_+} = -e^{-\bar{\omega}_-^2/4(1-\kappa^2)\sigma^2-\bar{t}_-^2\sigma^2}\frac{\bar{\omega}_-^2}{16\sigma^4}$. We can obtain the relation

$$\delta\bar{t}_-\delta\bar{\omega}_+ \geqslant 2\sqrt{1-\kappa^2}. \tag{D13}$$

[1] V. Giovannetti, S. Lloyd, and L. Maccone, Phys. Rev. Lett. **96**, 010401 (2006).
[2] V. Giovannetti, S. Lloyd, and L. Maccone, Nat. Photon. **5**, 222 (2011).
[3] M. Szczykulska, T. Baumgratz, and A. Datta, Adv. Phys.: X **1**, 621 (2016).
[4] J. Joo, W. J. Munro, and T. P. Spiller, Phys. Rev. Lett. **107**, 083601 (2011).
[5] M. Barbieri, PRX Quantum **3**, 010202 (2022).
[6] Z. Huang, C. Macchiavello, and L. Maccone, Phys. Rev. A **94**, 012101 (2016).
[7] N. Gisin and R. Thew, Nat. Photon. **1**, 165 (2007).
[8] A. Steane, Rep. Prog. Phys. **61**, 117 (1998).
[9] E. Knill, Nature (London) **463**, 441 (2010).
[10] B. P. Abbott, R. Abbott, T. D. Abbott, and M. R. Abernathy, Phys. Rev. Lett. **116**, 061102 (2016).
[11] R. Schnabel, N. Mavalvala, and P. K. Lam, Nat. Commun. **1**, 121 (2010).
[12] C. L. Degen, F. Reinhard, and P. Cappellaro, Rev. Mod. Phys. **89**, 035002 (2017).
[13] Z. Zhang and Q. Zhuang, Quantum Sci. Technol. **6**, 043001 (2021).
[14] J. M. Geremia, J. K. Stockton, A. C. Doherty, and H. Mabuchi, Phys. Rev. Lett. **91**, 250801 (2003).
[15] V. Giovannetti, S. Lloyd, and L. Maccone, Nature (London) **412**, 417 (2001).
[16] V. Giovannetti, S. Lloyd, L. Maccone, J. H. Shapiro, and F. N. C. Wong, Phys. Rev. A **70**, 043808 (2004).
[17] G. M. D'Ariano and L. Maccone, Electron. Notes Discret. Math. **20**, 133 (2005).
[18] M. A. Taylor and W. P. Bowen, Phys. Rep. **615**, 1 (2016).
[19] S.-H. Tan, B. I. Erkmen, V. Giovannetti, S. Guha, S. Lloyd, L. Maccone, S. Pirandola, and J. H. Shapiro, Phys. Rev. Lett. **101**, 253601 (2008).
[20] S. Barzanjeh, S. Guha, C. Weedbrook, D. Vitali, J. H. Shapiro, and S. Pirandola, Phys. Rev. Lett. **114**, 080503 (2015).
[21] J. H. Shapiro, IEEE Aerosp. Electron. Syst. Mag. **35**, 8 (2020).
[22] R. Nair and M. Gu, Optica **7**, 771 (2020).
[23] S. Guha and B. I. Erkmen, Phys. Rev. A **80**, 052310 (2009).
[24] Q. Zhuang and J. H. Shapiro, Phys. Rev. Lett. **128**, 010501 (2022).
[25] L. Maccone and C. Ren, Phys. Rev. Lett. **124**, 200503 (2020).
[26] G. Slepyan, S. Vlasenko, D. Mogilevtsev, and A. Boag, IEEE Antennas. Propag. Mag. **64**, 16 (2022).
[27] E. D. Lopaeva, I. Ruo Berchera, I. P. Degiovanni, S. Olivares, G. Brida, and M. Genovese, Phys. Rev. Lett. **110**, 153603 (2013).
[28] F. Xu, X.-M. Zhang, L. Xu, T. Jiang, M.-H. Yung, and L. Zhang, Phys. Rev. Lett. **127**, 040504 (2021).
[29] R. Demkowicz-Dobrzański, W. Górecki, and M. Guţă, J. Phys. A: Math. Theor. **53**, 363001 (2020).
[30] J. Liu, H. Yuan, X.-M. Lu, and X. Wang, J. Phys. A: Math. Theor. **53**, 023001 (2020).
[31] M. G. A. Paris, Int. J. Quantum Inf. **07**, 125 (2009).
[32] W. Heisenberg, Z. Phys. **43**, 172 (1927).
[33] P. Busch, T. Heinonen, and P. Lahti, Phys. Rep. **452**, 155 (2007).
[34] Q. Zhuang, Z. Zhang, and J. H. Shapiro, Phys. Rev. A **96**, 040304(R) (2017).
[35] Z. Huang, C. Lupo, and P. Kok, PRX Quantum **2**, 030303 (2021).
[36] M. Reichert, R. Di Candia, M. Z. Win, and M. Sanz, npj Quantum Inf. **8**, 147 (2022).
[37] M. Tsang, R. Nair, and X. M. Lu, Phys. Rev. X **6**, 031033 (2016).
[38] P. C. Humphreys, M. Barbieri, A. Datta, and I. A. Walmsley, Phys. Rev. Lett. **111**, 070403 (2013).
[39] L. Maccone, Y. Zheng, and C. Ren, arXiv:2309.11834.
[40] S. Yun, P. Xu, J. S. Zhao, Y. X. Gong, Y. F. Bai, J. Shi, and S. N. Zhu, Phys. Rev. A **86**, 023852 (2012).
[41] W.-T. Liu, P.-X. Chen, C.-Z. Li, and J.-M. Yuan, Phys. Rev. A **79**, 061802(R) (2009).
[42] R. Demkowicz-Dobrzański and L. Maccone, Phys. Rev. Lett. **113**, 250801 (2014).
[43] G. Arrad, Y. Vinkler, D. Aharonov, and A. Retzker, Phys. Rev. Lett. **112**, 150801 (2014).
[44] B. Escher, R. L. de Matos Filho, and L. Davidovich, Nat. Phys. **7**, 406 (2011).
[45] W. Górecki, A. Riccardi, and L. Maccone, Phys. Rev. Lett. **129**, 240503 (2022).
[46] T. Brougham, N. Samantaray, and J. Jeffers, Phys. Rev. A **108**, 052404 (2023).